Effective Wang-Teter kernels for improved orbital-free density functional theory simulations

Valeria Rios-Vargas,[1,*] Xuecheng Shao,[1,2,†] S. B. Trickey,[3,‡] and Michele Pavanello[1,2,§]

[1]*Department of Physics, Rutgers University, Newark, New Jersey 07102, USA*

[2]*Department of Chemistry, Rutgers University, Newark, New Jersey 07102, USA*

[3]*Quantum Theory Project, Department of Physics and Department of Chemistry, University of Florida, Gainesville, Florida 32611, USA*

(Received 8 May 2024; revised 16 July 2024; accepted 18 July 2024; published 12 August 2024)

We propose computationally cheap and accurate approximants to the noninteracting kinetic energy density functional $T_s[n]$ by leveraging the simplicity and computational efficiency of the Wang-Teter functional [L.-W. Wang and M. Teter, Phys. Rev. B **45**, 13196 (1992)]. It depends on a single parameter, the average electron density ρ_0. We address limitations of the Wang-Teter functional, which include variational instabilities and inability to treat materials with finite band gaps. We introduce three physically motivated methods for determining ρ_0: DEN, minimizing the integrated difference of the self-consistent Wang-Teter electron density from the one from conventional Kohn-Sham density functional theory (DFT); KIN, minimizing the deviation between the Wang-Teter $T_s[n]$ and the exact value from conventional Kohn-Sham DFT; and finally ENE, minimizing the difference between the Wang-Teter and conventional Kohn-Sham DFT total energies. The crucial result of this work is that our approaches effectively mitigate the drawbacks of the Wang-Teter functional. We provide a thorough analysis of our methods and discuss their potential for large-scale simulations and as templates for density-dependent nonlocal functionals.

DOI: 10.1103/PhysRevB.110.085129

I. INTRODUCTION AND BACKGROUND

Prediction of the electronic structure of materials and their molecular constituents is a task that underpins computational materials science [1]. In recent decades, many successes of electronic structure theory, and specifically of density functional theory (DFT) [2], have showcased its usefulness and objective predictive capabilities [3]. Unfortunately, the most commonly used formulation of DFT, i.e., conventional Kohn-Sham DFT (KS-DFT) in its orbital-dependent form, introduces a computational scaling of no less than N^3 where N is a measure of system size (e.g., the number of electrons in the system or the number of KS orbitals). This scaling arises from the need to diagonalize the KS Hamiltonian matrix. Therefore, the N^3 scaling is inescapable except in limiting cases such as extended metals at finite (high) temperature, extended systems with gap where the nearsightedness of the one-body reduced density matrix [4–6] can be exploited.

DFT and therefore KS-DFT are based on the realization that the electronic energy is strictly a functional of the electron density,

$$E[n] = T_s[n] + E_H[n] + E_{\rm xc}[n] + \int d\mathbf{r}\, v_{\rm ext}(\mathbf{r}) n(\mathbf{r}), \quad (1)$$

where the external potential is indicated by $v_{\rm ext}(\mathbf{r})$, the classical electron-electron repulsion (Hartree) is E_H, and the exchange-correlation functional (which collects the quantum corrections to the electron-electron repulsion along with the correlational kinetic energy) is $E_{\rm xc}$.

The working expression of conventional KS-DFT, the KS equation, is an eigenvalue equation for the so-called KS orbitals $\phi_i[n](\mathbf{r})$:

$$\left[-\tfrac{1}{2}\nabla^2 + v_s[n](\mathbf{r})\right]\phi_i[n](\mathbf{r}) = \epsilon_i \phi_i[n](\mathbf{r}). \quad (2)$$

The KS potential is given by

$$v_s[n](\mathbf{r}) = \frac{\delta E_H[n]}{\delta n(\mathbf{r})} + \frac{\delta E_{\rm xc}[n]}{\delta n(\mathbf{r})} + v_{\rm ext}(\mathbf{r}). \quad (3)$$

The kinetic energy of noninteracting electrons $T_s[n]$ depends explicitly on the one-electron KS orbitals (in positive-definite form)

$$T_s[n] = \frac{1}{2}\sum_i f_i \langle \nabla\phi_i | \nabla\phi_i \rangle, \quad (4)$$

where the occupation numbers f_i are such that $\sum_i f_i = N$ and are either Aufbau or follow the Fermi-Dirac distribution, where N is the number of electrons. The electron number density itself is

$$n(\mathbf{r}) = \sum_i f_i |\phi_i(\mathbf{r})|^2. \quad (5)$$

Hence, T_s depends implicitly on the electron density.

As mentioned before, the orthogonalization of the KS orbitals causes the calculation cost to scale like $O(N^3)$. On the other hand, orbital-free DFT (OF-DFT), while based on exactly the same theoretical framework as conventional KS-DFT is, in effect, an alternative to it. OF-DFT exploits a

*Contact author: valeria.rios@rutgers.edu
†Contact author: xuecheng.shao@rutgers.edu
‡Contact author: trickey@ufl.edu
§Contact author: m.pavanello@rutgers.edu

 ©2024 American Physical Society

fundamental result of DFT, namely, that all the ground-state observables can in principle be calculated from the electronic density alone. That includes the noninteracting kinetic energy T_s. To find the electronic density that minimizes the energy, in OF-DFT one must minimize the KS-DFT Lagrangian as an explicit density functional, to wit

$$\mathcal{L}[n] = E[n] - \mu\left(\int n(\mathbf{r})d\mathbf{r} - N\right). \tag{6}$$

The last term ensures proper normalization.

Carrying out such a minimization is computationally advantageous provided that, first, an accurate explicit form is known for $T_s[n]$, and, second, that evaluation of that approximate $T_s[n]$ is computationally cheap. Thus, in OF-DFT, $T_s[n]$ is approximated by pure density functionals whose evaluation cost is kept at or under $O[N\ln(N))]$. See Ref. [7] for details. Briefly, in 1927, the local density approximation to $T_s[n]$ led to the Thomas-Fermi kinetic energy T_{TF} [8]. Explicitly, it is

$$T_{\mathrm{TF}}[n] = c_{\mathrm{TF}}\int d\mathbf{r}\, n^{\frac{5}{3}}(\mathbf{r}) \equiv \int d\mathbf{r}\, \tau_{\mathrm{TF}}(\mathbf{r}) \tag{7}$$

with $c_{\mathrm{TF}} := \frac{3}{10}(3\pi^2)^{2/3}$. In 1935 von Weizsäcker developed a gradient correction T_{vW} [9]. Explicitly. it is

$$T_{\mathrm{vW}}[n] := \frac{1}{2}\int d\mathbf{r}\, \nabla\sqrt{n(\mathbf{r})}\cdot\nabla\sqrt{n(\mathbf{r})}. \tag{8}$$

It was followed up in the 1990s with the so-called generalized gradient approximations (or GGAs) [10] which continue to be developed today [11–13].

Kinetic energy density functionals (KEDFs) also can be formulated to have a nonlocal dependence on the electron density. They usually are developed starting from the ansatz

$$T_s[n] = T_{\mathrm{TF}}[n] + T_{\mathrm{vW}}[n] + T_{\mathrm{NL}}[n], \tag{9}$$

where the nonlocal contribution of the KEDF has the generic form

$$T_{\mathrm{NL}}[n] = \int d\mathbf{r}\int d\mathbf{r}' n^{\alpha}(\mathbf{r})\omega[n](\mathbf{r},\mathbf{r}')n^{\beta}(\mathbf{r}'). \tag{10}$$

Here α and β are positive scalars, and ω is a kernel function of dimension $(1/\mathrm{length})^w$ with $w = 8 - 3(\alpha+\beta)$ that relates kinetic energy densities at any two spatial points $\mathbf{r}$ and $\mathbf{r}'$.

The challenge is to find an appropriate kernel for nonlocal functionals. The guiding principle in functional development has been to satisfy as many exact conditions as possible [14,15]. In particular, exact conditions in the limit of the homogeneous electron gas (HEG) have been important for applications of OF-DFT to materials science problems [7,16–19].

The details of kernel development begin with the relationship of the second functional derivative of the KEDF with the KS static response function, namely,

$$\frac{\delta^2 T_s[n]}{\delta n(\mathbf{r})\delta n(\mathbf{r}')} = -\chi_s^{-1}(\mathbf{r},\mathbf{r}'). \tag{11}$$

Discussion of this relationship is in Ref. [7].

In the HEG limit, the KS response function has a simplified relation (given by Lindhard) in reciprocal space ($\eta = \frac{q}{2k_F}$ is a dimensionless momentum and q is the reciprocal variable to $|\mathbf{r}-\mathbf{r}'|$) [20]:

$$\chi_{\mathrm{Lind}}(\eta) = -\frac{k_F}{\pi^2}\left[\frac{1}{2} + \frac{1-\eta^2}{4\eta}\ln\left|\frac{1+\eta}{1-\eta}\right|\right], \tag{12}$$

where $k_F = (3\pi^2\rho_0)^{1/3}$ is the Fermi wave vector for the HEG with electron density $\rho_0 = \frac{N}{V}$, and N is the number of electrons in the cell of volume V. The incorporation of the linear response theory in the derivation of the kernel plays an important role for describing the oscillations of the density in the short-range and the Friedel oscillations for metals [21].

The connection, Eq. (11), between Eqs. (12) and (10) can be exploited easily by inverting the Lindhard function and arriving at a kernel of the kind $\omega(\mathbf{r},\mathbf{r}') = \omega(|\mathbf{r}-\mathbf{r}'|)$. This can be expressed more conveniently in reciprocal space,

$$\hat{\mathcal{F}}\omega(\mathbf{r}-\mathbf{r}') = \tilde{\omega}(\mathbf{q}) = -\frac{\chi_{\mathrm{Lind}}^{-1} - \chi_{\mathrm{vW}}^{-1} - \chi_{\mathrm{TF}}^{-1}}{2\alpha\beta c_{\mathrm{TF}}\rho_0^{\alpha+\beta-2}}, \tag{13}$$

where $\hat{\mathcal{F}}$ is the Fourier transform with respect to $|\mathbf{r}-\mathbf{r}'|$.

Whether the optimal choice of ρ_0 is as the average density (i.e., $\rho_0 = N/V$) is an obvious question. From early in the development of KEDFs [16], it was recognized that this choice is undefined for many systems of interest (e.g. molecules, surfaces). Typically, ways to circumvent that limitation were used. The focus of this work, instead, is precisely to exploit the freedom to choose ρ_0 in the setting of real material simulations.

Before discussing kernel density dependence, however, we note that approximations to Eq. (13) can be devised in terms of polynomials of q/k_F. Examples include truncation at second order or in a generalized fashion akin to GGAs to give rise to Laplacian-level KEDFs [22]. Those give rise to KEDFs that have response properties that can be similar to nonlocal functional response even though they miss the logarithmic singularity at $q = 2k_F$ [23].

As indicated in Eq. (10), the kernel function itself should be a density functional, not simply a spatial function. Thus, it should have pointwise density dependence, not merely the constant average number density in the simulation cell in Eq. (13). The question of what specific density dependence should be in an approximate kernel has drawn the attention of the OF-DFT community for decades. There are, nonetheless, many examples of nonlocal KEDFs with density-independent kernels that can be implemented efficiently and applied to materials science problems. These include Wang-Teter (WT) [17], Wang-Govind-Carter (WGC) [16,24], Perrot [19], and Smargiassi-Madden (SM) [18], Mi-Genova-Pavanello (MGP) [25], and KGAP of Della Sala and coworkers [26].

KEDFs with density-dependent kernels have been developed based on the idea that the Fermi wave vector in the Lindhard function can be approximated by a locally density dependent one, specifically $k_F(\mathbf{r}) = [3\pi^2 n(\mathbf{r})]^{1/3}$. Several functionals employ that approximation, for example, the LMGP functional [27,28], Huang-Carter (HC) [29], and revHC (an alternative to HC that avoids some of its numerical and computational complications [30]).

Another line of functionals, WGC99 [16], XWM [31], and CAT [32], improve upon the previously mentioned approach by the use of a more physical density dependence of

the kernel. They employ an effective nonlocal Fermi wave vector of the type $\tilde{k}_F(\mathbf{r},\mathbf{r}') = (\frac{k_F^\gamma(\mathbf{r})+k_F^\gamma(\mathbf{r}')}{2})^{1/\gamma}$. Unfortunately, the computational cost associated with such nonlocal Fermi wave vectors limits the applicability of such functionals to systems that are close to the HEG. See Ref. [7] and references therein for a discussion of this point in relation to a numerically challenging Taylor expansion.

As the foregoing summary shows, nonlocal KEDFs with density-independent kernels have an advantage over KEDFs with density-dependent kernels in terms of simplicity and, therefore, computational cost. The problem, however, that arises with this type of functionals already has been noted: there is no manifestly preferable prescription for choosing the reference density ρ_0. Given that, the application of such functionals to systems with quite inhomogeneous electron densities is particularly striking. Even more problematic is the mathematically exact finding by Blanc and Cancs [33] (hereafter "BC instability") that a WT-like kernel (with $\rho_0 = N/V$) results in variationally unstable functionals. Such instability was characterized later by Witt *et al.* [34] and also discussed in Ref. [7].

Taking into account the complexities outlined above, here we propose that employment of constraint-based ρ_0 values can yield significantly enhanced performance of a density-independent kernel functional compared to the conventional $\rho_0 = N/V$ choice. In particular, we show that these pragmatic ρ_0 values actually broaden the applicability of the Wang-Teter functional to include semiconductors, such as the CD (cubic diamond) and dhcp (double hexagonal-close-packed) phases of Si. Furthermore, we illustrate that utilization of pragmatic ρ_0 values allows us to circumvent the BC instability in practice. Consequently, our work presents an approach for determining the value of ρ_0 tailored specifically for nonlocal KEDFs with density-independent kernels. The relevance of insights gained from this study to the broader class of KEDFs with density-dependent kernels is a matter for future exploration.

II. METHODS

Several studies have used some sort of empirically determined ρ_0, either based on the bulk value [21] or optimized to reproduce the equation of state (EOS) on a system-dependent basis [25]. To our knowledge, what has not been done is to calibrate ρ_0 to some conventional KS-DFT quantity, thereby exploiting the underlying commonality of the two. We focus here on the WT functional and consider four effective ρ_0 which we denote as DEN, KIN, ENE, and AVE. These are found by carrying out the following operations independently of the materials of interest:

DEN: Minimization of the density difference between the OF-DFT density, $n_{\rm OF}(\mathbf{r})$, and the conventional KS-DFT density, $n_{\rm KS}(\mathbf{r})$,

$$\rho_0 = \underset{\rho_0}{\rm argmin}\frac{1}{2}\int |n_{\rm OF}(\mathbf{r}) - n_{\rm KS}(\mathbf{r})| d\mathbf{r}. \tag{14}$$

(The factor $\frac{1}{2}$ is included to correct for a double counting, as the integral of an absolute value sums both the positive and negative portions of a function.)

KIN: Minimization of the difference between the T_s values for OF-DFT, $T_{\rm OF}$, and conventional KS-DFT, T_s, evaluated with the conventional KS density,

$$\rho_0 = \underset{\rho_0}{\rm argmin}|T_s[n_{\rm KS}] - T_{\rm OF}[n_{\rm KS}]|. \tag{15}$$

.

ENE: Minimization of the difference between the total OF-DFT energy, $E_{\rm OF}$, and the total energy from conventional KS-DFT, $E_{\rm KS}$, evaluated at their respective self-consistent electron densities,

$$\rho_0 = \underset{\rho_0}{\rm argmin}|E_{\rm KS}[n_{\rm KS}] - E_{\rm OF}[n_{\rm OF}]|. \tag{16}$$

AVE: $\rho_0 = \frac{N}{V}$, the usual choice for the WT functional.

We note immediately that neither AVE nor any of three constraint-based choices of ρ_0 resolve the WT violation of the uniform density scaling condition [35] (see Appendix A), namely,

$$T_s[n_\lambda] = \lambda^2 T_s[n], \quad n_\lambda(\mathbf{r}) = \lambda^3 n(\lambda\mathbf{r}). \tag{17}$$

That violation is intrinsic to the WT functional because the α and β exponents in it are $\alpha + \beta = \frac{5}{3}$. As noted already, dimensional analysis shows that they should sum to $\frac{8}{3}$.

In testing the four options, we compare against various Si phases, such as CD (cubic diamond) and DHCP (double HCP) which have finite band gap. Also BCC (body-centered cubic), fcc (face-centered cubic), HCP (hexagonal close-packed), BCT5 (body-centered tetragonal, type 5), SH (simple hexagonal), and β tin which exhibit a significant electronic density of states at the Fermi level and thus are metallic.

For each of these phases we compute the usual equilibrium parameters, such as the total electronic energy at the equilibrium lattice constant E_0, the equilibrium volume V_0, and the bulk modulus B_0. In practice, we run a finite set of single-point calculations and then we fit the resulting energy vs lattice constant curve with a third-order inverse polynomial [36].

In addition, we compute the elastic moduli for CD Si by fitting the primitive cell energy-versus-strain curves with second-order polynomials. Specifically, we calculate four elastic moduli (which represent orthorhombic, uniaxial, and triaxial deformations), C', C_{11}, C_{12}, and C_{44}, following the procedures outlined in Refs. [37,38].

We also compute static response properties according to the harmonic perturbation approach introduced earlier by Moldabekov *et al.* [23], as well as the "lesser" Fukui function f_- [39]. The Fukui function is a local measure of reactivity and the perturbation approach considered here is a measure of particle-conserving response. Thus, they represent quite strenuous tests of a parametrization such as our proposed prescriptions for ρ_0.

The harmonic response was computed by applying the external potential

$$v_{\rm appl}(\mathbf{r}) = A\,\cos(\mathbf{k}\cdot\mathbf{r}). \tag{18}$$

In it, the direction of $\mathbf{k}$ is arbitrary but its components must satisfy the periodicity requirements of the system. That is, along each lattice vector direction, the allowed values of $\mathbf{k}$ are $k_a = \frac{2\pi n_a}{a}$ along the a direction with $n_a = 1, 2, \ldots$, and similarly along b and c. We choose the strength of the perturbation to be $A = 0.01$ Ha. In our simulations we use $n_a = 1$ to probe

the "low-q" density response and $n_a = 5$ for the "high-q" response.

The Fukui function is defined as the derivative of the electron density with respect to the total number of electrons, namely,

$$f_\pm = \frac{d\, n[N](\mathbf{r})}{dN_\pm} = \lim_{h\to 0} \frac{n[N \pm h](\mathbf{r}) - n[N](\mathbf{r})}{\pm h}. \tag{19}$$

The plus-minus distinction arises because of the derivative discontinuity at integer N in DFT. In practice, we use $h = 0.1$ and we report the Hartree self-energy of the Fukui functions as follows:

$$H_f = \int \frac{[f_-(\mathbf{r}) - 1][f_-(\mathbf{r}') - 1]}{|\mathbf{r} - \mathbf{r}'|} d\mathbf{r}, \tag{20}$$

which we can evaluate in reciprocal space given that $\int [f_-(\mathbf{r}) - 1] d\mathbf{r} = 0$, thus avoiding the $G = 0$ singularity.

III. COMPUTATIONAL DETAILS

Conventional KS calculations and OF-DFT simulations were performed using QEPY [40] and DFTPY [41], respectively, with bulk-derived local pseudopotentials (BLPS) [42]. In addition, all calculations used the local density approximation (LDA) for electron exchange correlation [43]. The energy cutoff established for all OF-DFT calculations was 680 eV and, for the orbitals in conventional KS calculations, was set to 816 eV. The first Brillouin zone was sampled by $20\times20\times20$ k points as in Monkhorst-Pack grids [44,45].

The values in the tables are determined by Python scripts that use DFTPY and QEPY. The scripts to recover all figures and tables in this work are collected in a static snapshot of a GitHub repository available on GitHub [46].

IV. RESULTS

For each of the phases of Si considered, Table I reports the equilibrium parameters computed from both conventional KS-DFT and OF-DFT with the WT functional for each of the choices of ρ_0 discussed previously. Specifically, we present the equilibrium volume (V_0), equilibrium total energy per atom (E_0), and bulk modulus (B_0). ρ_0 parameters for the equilibrium structures are presented in Table II. Focusing on the equilibrium volume V_0, we notice that in almost all cases, the WT functional with the three constraint-based ρ_0 values (DEN, KIN, and ENE) outperforms the usual choice (AVE). Although for the metallic phases the improvement from the constraint-based ρ_0 values over AVE is modest (2%–5%), for the semiconducting phases only the constraint-based ρ_0 deliver stable phases. AVE for CD, DHCP, and SH wrongly predicts unbound systems.

The bulk modulus B_0 generally follows the same behavior as V_0 with some notable deviations. The AVE values for B_0, for example, are either severely underestimated or severely overestimated. DEN, ENE, and KIN results, instead, are all generally much closer to the conventional KS reference values.

The equilibrium energy E_0 also shows that the constraint-based ρ_0 values deliver much improved phase energy ordering. For example, AVE puts β-tin above BCC while in fact it should be below. Unfortunately, the energy E_0 calculated with DEN deviates by about 0.6 eV from the KS reference for BCT5, above the bcc phase energy. However, we note that the DEN, KIN, and ENE choices improve outcomes greatly over the AVE results. In Fig. 1 we provide a visualization of the energy versus volume behavior for CD and BCC. It shows the strikingly unphysical outcome caused by AVE even when there appears to be an energetic local minimum such as for

TABLE I. Equilibrium parameters (equilibrium energy E_0, equilibrium volume V_0, and bulk modulus B_0) calculated for each phase by fitting energy vs volume, $t \in [0.8, 1.4]$ (see caption of Fig. 1 for details). We report values for several phases of silicon and for the four choices of the ρ_0 parameter of the WT kernel. Energies are referenced to the equilibrium energy of the CD phase. Conventional KS-DFT values (indicated by KS) are also reported for comparison. AVE is given as "–" for SH, CD, and DHCP because for these phases WT with AVE ρ_0 values predicts unbound crystals.

Si phase	ρ_0	V_0 (Å^3/atom)	E_0 (meV/atom)	B_0 (GPa)
β-tin	KS	14.800	119	116.8
	KIN	14.935	153	113.9
	ENE	14.801	119	116.8
	DEN	14.629	57	140.8
	AVE	14.447	365	88.9
BCC	KS	14.338	285	100.5
	KIN	14.488	319	98.5
	ENE	14.326	279	102.2
	DEN	14.291	189	117.9
	AVE	14.706	393	55.6
FCC	KS	13.760	300	102.8
	KIN	13.905	338	99.6
	ENE	13.760	300	102.8
	DEN	13.546	222	123.2
	AVE	14.916	416	48.0
HCP	KS	14.138	260	100.9
	KIN	14.289	298	98.3
	ENE	14.142	261	100.8
	DEN	14.094	171	119.4
	AVE	14.347	412	58.3
SH	KS	14.589	120	117.4
	KIN	14.716	152	114.8
	ENE	14.589	120	117.4
	DEN	14.247	60	147.8
	AVE	–	–	–
BCT5	KS	16.953	177	100.8
	KIN	17.078	193	99.3
	ENE	16.953	177	100.8
	DEN	16.228	305	137.7
	AVE	17.375	704	36.5
CD	KS	19.892	0	88.7
	KIN	19.997	0	88.0
	ENE	19.891	0	88.7
	DEN	19.672	0	98.0
	AVE	–	–	–
DHCP	KS	19.776	9	90.1
	KIN	19.882	10	89.3
	ENE	19.775	9	90.1
	DEN	18.564	305	119.4
	AVE	–	–	–

TABLE II. Parameter ρ_0 in Hartree atomic units for the equilibrium structure of all Si phases considered. All values should be multiplied by 10^{-2}.

	KIN	ENE	DEN	AVE
β-tin	3.49169	3.51565	3.65791	3.86712
BCC	5.62952	5.64018	5.69329	6.00582
FCC	4.79818	4.82134	4.49756	4.01807
HCP	2.17497	2.29267	2.2831	2.96179
BCT5	2.21286	2.34529	2.63874	3.01834
SH	4.20006	4.21712	4.33257	4.27526
CD	2.79672	2.88202	4.69511	3.50586
DHCP	3.61805	3.63498	3.75672	3.38523

BCC. Finally, we note that for the DHCP phase DEN correctly predicts a bound state, and places its energy above that of CD even though the energy is greatly overestimated. Overall, ENE provides the best agreement against conventional KS-DFT. This comes at no surprise, as ENE is constructed to reproduce the total energy. Second in energy performance is KIN and then DEN.

We also check the performance of the KEDFs for the calculation of elastic moduli of CD Si (see Table III). KIN, ENE, and DEN outperform the conventionally employed AVE. Particularly, KIN and ENE (although ENE does so by construction) demonstrate a superior capability for describing the strain deformation of CD Si. These results are extremely important as they show the ability of all the proposed methods to reproduce the energetics of CD Si for strains inducing strong perturbation of the directional character of the Si-Si bonds.

In Fig. 2 we display the OF-DFT density difference against conventional KS-DFT for the four choices of ρ_0 for the BCT5 phase of silicon. We showcase this phase as it provides the most insightful depiction of the density difference compared to the other phases. All the constraint-based ρ_0 choices, KIN, ENE, and DEN, provide clear improvements over the usual ρ_0 value, AVE. The density improvements are most obvious in the interstitial region, a fact directly correlated to chemical bonding. This figure provides us with an indication that not only DEN, but also KIN and ENE are associated with a generally improved predicted electronic structure over AVE.

In an effort to probe physical conditions under which the satisfaction of density scaling conditions may play a crucial

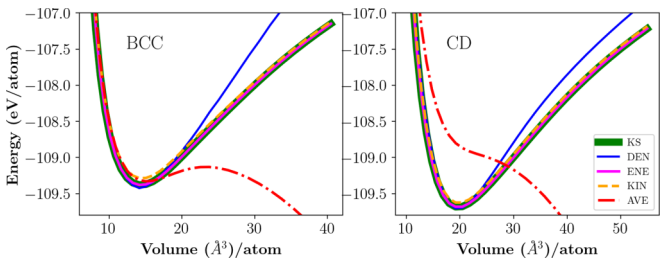

FIG. 1. Energy vs volume computed with all KEDFs considered along a path that conserves the cell symmetry, i.e., volume scaling $V_t = t^3 V$ where t is a scaling factor for $t \in [0.8, 1.4]$ for bcc and CD phases of silicon.

TABLE III. Elastic constants of CD Si reported in Mbar. A "–" is reported for AVE for those constants requiring the bulk modulus (see Table I). See text for additional details.

	KIN	ENE	DEN	AVE	KS
C'	0.579	0.514	0.438	0.155	0.520
C_{44}	0.655	1.025	0.659	0.371	1.022
C_{11}	1.798	1.980	1.188	–	1.966
C_{12}	0.640	0.952	0.312	–	0.926

role, in Tables IV and V, we report RMSDs for the total energy and noninteracting kinetic energy along a volume scaling path (see table captions). For the total energy, we notice that even though ENE performs best by construction, the other constraint-based ρ_0 choices also perform very well and much better than the AVE. The RMSDs in Table IV were obtained with self-consistent densities. In contrast, the results in Table V were computed with the conventional KS electron density. Thus, they identify functional-driven error only [47]. Clearly, as the focus in that table is the kinetic energy, KIN performs best. However, both DEN and ENE improve drastically on the AVE results. We notice that the largest deviations for DEN and ENE are recorded for the semiconducting phases CD and DHCP.

For better visualization of the effects of the volume scaling on the KEDF, in Fig. 3 we plot the Pauli kinetic energy ($T_P = T_s - T_{\rm vW}$) as a function of the volume scaling factor t for the CD phase of Si. We choose the range $1 < t < 3$ which is wider than the one used for Tables IV and V. The Pauli energy should be bound and positive semidefinite [7,48], $T_P \geqslant 0$. We point out that all of the constraint-based ρ_0 values cause the Pauli kinetic energy to converge to an asymptote in the isolated atom limit (i.e., large-t values) while use of AVE incorrectly plunges T_P into negative values, an unphysical behavior [7,33,34]. The constraint-based ρ_0 values do not specifically encode Pauli energy positivity. However, the result from Fig. 3 is not completely unexpected as we expect the ρ_0 values of DEN, KIN, and ENE to reach an asymptote in the isolated atom limit, delivering a T_P necessarily bounded from below.

Figure 3 also includes results from a functional version called SCA. It is a variant of the WT functional whose kernel from Eq. (13) is modified to scale properly like Eq. (17) in the following way (see Appendix A):

$$\tilde{\omega}_{\rm SCA}(\mathbf{q}) = \frac{N}{V\tilde{\rho}_0}\tilde{\omega}(\mathbf{q}), \tag{21}$$

where $\tilde{\rho}_0$ is a constant such that $\tilde{\rho}_0 = N/V_0$, where V_0 is chosen to be the equilibrium volume of the CD phase of Si.

Clearly, SCA is an *ad hoc* modification of the WT functional which we do not explore further here. Here SCA serves the purpose of explaining the link between correct scaling of a KEDF and its physical and unphysical behavior as a function of the volume scaling factor t. In particular, we notice in Fig. 3 that, as with ENE, DEN, and KIN, SCA correctly reaches an asymptote for T_P in the isolated atom limit, thereby avoiding Pauli energy negativity. That is at the source of the BC instability [7,34]. We stress, however, that Pauli energy positivity

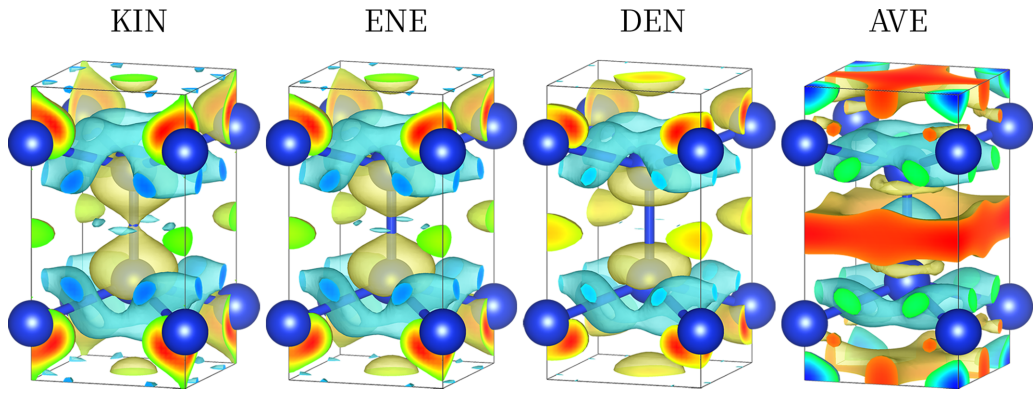

FIG. 2. Difference of the OF-DFT density from the conventional KS-DFT density for BCT5 silicon at the experimental lattice constant. The ρ_0 parameters used are reported in Table II. The same isosurface cutoff of 0.01 was employed for the four cases [yellow (blue) represent positive (negative) values].

cannot be ensured with the constraint-based ρ_0 values. What can be ensured is that the Pauli energy will be bounded from below.

In the Supplemental Material, Table S1 [49], we report the H_f measure of the lesser Fukui function (see Methods section for details). We notice that the results are dependent on the choice of ρ_0, showing that OF-DFT predictions from functionals of the type considered here are good for metals but less so for semiconductor phases. Among the methods considered, KIN probably performs best, even though only incrementally. Examination of Fukui function results alone might suggest that the choice AVE gives similar results as KIN, DEN and ENE. But that needs to be contextualized considering the gross failure of AVE to yield proper structures. Nevertheless, the Fukui functions predicted by KIN, ENE, and DEN are useful for comparison of trends. The actual values are not quantitatively accurate, a reminder of how difficult it is to get accurate local quantities from a comparatively simple kernel for nonlocal KEDFs.

In Tables VI and VII, we present the results of the electron density response due to an external perturbation of the kind in Eq. (18) (see Supplemental Material, Tables S2 and S3 for the energy response and S4 and S5 [49] for the KEDF response). As mentioned before, we probe two regimes, high q and low q (see Methods for details). The low-q perturbation probes long-range responses which should be well captured by orbital-free density functionals [23] for metallic systems. For semiconductors (like CD and dhcp), the low-q limit of the inverse Lindhard function employed in the WT functional is incorrect (i.e., it tends to a constant while instead it should go like $1/q^2$, see Ref. [29]) and therefore one would expect strong deviation in the predicted responses in this limit. The high-q response probes the high-q limit of the WT kernel which is the same for all (reasonable) choices of ρ_0.

Tables VI and VII show that the OF-DFT results are in generally qualitative agreement with the conventional KS-DFT results. The agreement is not broken by the AVE ρ_0 results which fall in line with the outcomes of the other three ρ_0 choices. Surprisingly, the low-q response for the semiconductor phases, CD and DHCP, is in generally good agreement with the conventional KS-DFT response. Similar behavior was observed in a prior study [23], likely attributed to the utilization of simulation cells with relatively small dimensions that inhibit the exploration of very low values of $\mathbf{k}$ in Eq. (18).

Additionally, we address a crucial exact condition for a KEDF, namely, the reduction to the von Weizsäcker

TABLE IV. Root-mean-square deviation (RMSD) of the total electronic energy (in eV/atom) along a linear path (volume scaling) such that the lattice vectors and ionic positions are defined as, in crystal coordinates, $[a_t, b_t, c_t] = [ta_0, tb_0, tc_0]$ with $t \in [0.8, 1.4]$ for several phases of silicon and for the four choices of the ρ_0 parameter in the WT kernel. The self-consistent electron density was used in each case.

	KIN	ENE	DEN	AVE
β-tin	0.008	0	0.395	1.439
BCC	0.009	0	0.18	1.357
FCC	0.018	0	0.022	0.151
HCP	0.009	0	0.163	0.986
BCT5	0.006	0	0.847	1.925
SH	0.008	0	0.315	1.131
CD	0.004	0	0.052	3.321
DHCP	0.005	0	0.446	3.027

TABLE V. Root-mean-square deviation (RMSD) of the noninteracting kinetic energy (in eV/atom) T_s along the volume scaling path described in Table IV. The conventional KS electron density is employed in all cases. A value of 0 is given for values less than 1.0×10^{-3}.

	KIN	ENE	DEN	AVE
β-tin	0	0.501	0.112	1.577
BCC	0	0.462	0.15	1.659
FCC	0	0.061	0.017	0.225
HCP	0	0.379	0.106	1.403
BCT5	0	0.709	0.145	1.698
SH	0	0.451	0.095	1.426
CD	0	1.260	1.110	2.006
DHCP	0	1.063	0.681	1.776

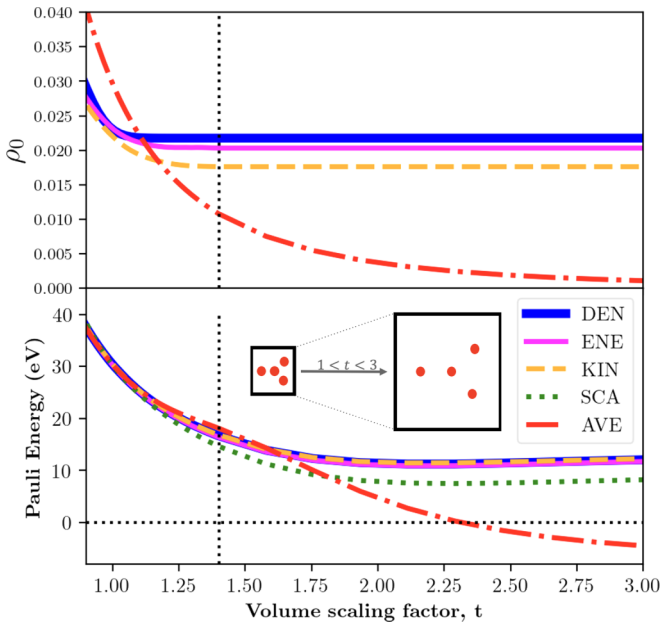

FIG. 3. Pauli energy ($T_P = T_s - T_{\rm vW}$, where T_s is taken from the value of the WT functional evaluated with the ρ_0 given by the methods indicated in the legend) as a function of t for $1 < t < 3$ for the CD phase of Si. A depiction of the behavior of cell and ion positions as a function of the volume scaling factor t is provided as inset.

potential for one- and two-electron systems. In Fig. 4, we present plots of the KEDF potential $v(\mathbf{r}) = \frac{\delta T_s}{\delta n(\mathbf{r})}$, computed using the conventional KS density for various functionals applied to helium, a two-electron atom [for ease of visualization, we report the product of $v(\mathbf{r})$ with $n(\mathbf{r})$]. The figure illustrates that virtually all WT-like functionals (KIN, ENE, and DEN) exhibit similar behavior in this limiting case. Generally, they underestimate the potential strength in the atomic region. Conversely, the GGA functional LKT tends to overestimate the potential. As previously reported [27], LMGP exhibits close agreement with vW.

Table S6 in the Supplemental Material [49] provides the Pauli energy values ($T_s[n] - T_{\rm vW}[n]$ or $T_{\rm TF}[n] + T_{\rm NL}[n]$ for nonlocal KEDFs) revealing that KIN inherently yields a null Pauli energy. That is followed by LMGP, DEN, ENE, and LKT. Remarkably, DEN and ENE exhibit negative Pauli

TABLE VI. Low-q density response [$n_a = 1$ in Eq. (18)]. The reported values measure the departure of the response density from the ground-state density $\frac{1}{2A}\int |n_{\rm resp}(\mathbf{r}) - n(\mathbf{r})| d\mathbf{r}$.

	KIN	ENE	DEN	AVE	KS
β-tin	2.014	2.018	2.012	2.008	2.023
BCC	3.258	3.256	3.293	3.373	3.556
FCC	2.180	2.180	2.177	2.164	2.197
HCP	1.869	1.870	1.860	1.861	1.928
BCT5	3.623	3.596	3.537	3.464	3.354
SH	2.113	1.919	2.152	2.108	1.889
CD	2.123	2.113	2.113	2.073	1.921
DHCP	3.785	3.744	3.660	3.569	3.423

TABLE VII. High-q density response [$n_a = 5$ in Eq. (18)]. The reported values measure the departure of the response density from the ground-state density $\frac{1}{2A}\int |n_{\rm resp}(\mathbf{r}) - n(\mathbf{r})| d\mathbf{r}$.

	KIN	ENE	DEN	AVE	KS
β-tin	0.980	0.981	0.980	0.983	0.983
BCC	0.378	0.378	0.378	0.378	0.388
FCC	0.471	0.471	0.471	0.471	0.469
HCP	0.415	0.416	0.407	0.405	0.402
BCT5	0.446	0.446	0.445	0.445	0.443
SH	0.501	0.695	0.432	0.479	0.448
CD	1.312	1.311	1.311	1.308	1.299
DHCP	0.562	0.561	0.560	0.560	0.556

energy, a phenomenon previously avoided in Si phases but generally unavoidable unless explicitly enforced in the defining equations for the method (see DEN, KIN, ENE definitions in the Methods section). However, as observed in Si phases under volume scaling, the effective ρ_0 values lead to a an asymptotic value in the isolated atom limit. Hence, we do not anticipate variational instability (i.e., BC instability) in the KEDF.

Let us analyze this point further. In the isolated atom limit for helium, DEN is tasked with achieving a vanishingly small Pauli potential. Without a null Pauli potential, the density predicted by DEN cannot match the KS density. Unfortunately, a WT-like KEDF never can achieve an exactly null Pauli potential. As can be seen in Appendix B, the best WT can do to minimize the Pauli potential is to explore the $\rho_0 \to 0$ limit where any η [or q, see Eq. (12)] dependence is removed (as can be seen in the Appendix, terms of $\frac{1}{\eta^2}$ and beyond would vanish in the limit of $\rho_0 \to 0$). In this limit, the Pauli potential from WT-like KEDFs tends to -0.28 of

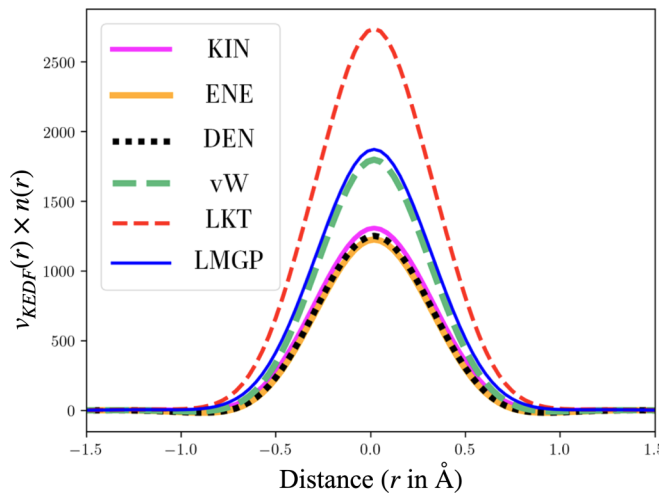

FIG. 4. For the helium atom, the von Weizsäcker potential is also the exact noninteracting kinetic energy potential $\frac{\delta T_s}{\delta n(\mathbf{r})} = v_{\rm vW}(\mathbf{r})$. The plot features the density times the potential for the three WT-like functionals (KIN, ENE, and DEN) as well as LMGP [27] and LKT [11]. AVE WT-like functional is not included as AVE ρ_0 values are not well defined for isolated systems, like atoms.

Thomas-Fermi, violating Pauli positivity. Our results for helium in Table S7 [49] show a Pauli energy for DEN of −0.651 Ha which corresponds to −0.279 Thomas-Fermi for this system.

V. DISCUSSION AND CONCLUSION

We have explored the possibility of tuning the kernel of the nonlocal part of the Wang-Teter functional by employing a constraint-based value of the ρ_0 parameter. Our strategy is to depart from choosing ρ_0 as the average number of electrons in the simulation cell. Rather, we choose a ρ_0 that minimizes the error against some quantity from conventional Kohn-Sham DFT. We present three options that minimize the error of (1) density, (2) noninteracting kinetic energy, and (3) total electronic energy.

The resulting methods were tested against several benchmarks aimed at assessing different aspects of the quality of the electronic structure (from the equation-of-state parameters, strain, to the density response to external static perturbations, the quality of the predicted lesser Fukui function to the behavior in the limiting case of a two-electron system). From the tests there emerges the clear conclusion that the constraint-based ρ_0 choices are superior to the commonly employed average number of electrons over the simulation cell.

Our results show that even a simple nonlocal functional with density-independent kernel can be made almost accurate by physically and formally sensible choice of its one free parameter. While the energy ordering of the silicon phases still is not exact, it is much improved. For example, CD and dhcp are the most stable phases and SH and β-tin are similar in energy. In comparison, WT predicts CD, DHCP, and SH to be unbound. Another important aspect of these methods is their ability to correctly describe the CD Si phase under strain (including orthorhombic, uniaxial, and triaxial). The results show that as the strain probes against the directional character of the Si-Si bonds, the traditional AVE is unable to provide qualitatively good results. Conversely, the three proposed methods recover the correct trends quantitatively in the case of ENE and semiquantitatively in the cases KIN and DEN.

Additional, major improvements to the WT functional given by the constraint-based ρ_0 choices include the correction of the BC instability in the isolated atom limit. This is the reason behind the functionals predicting, correctly, bound phases for CD, DHCP, and SH. In regards to the BC instability, we showed that the constraint-based choices of ρ_0 necessarily provide asymptotically converged ρ_0 values as a function of increasing lattice constant (i.e., the isolated atom limit will be met with a constant and nonzero ρ_0 regardless of the specific choice). This leads to maintaining bound (finite) Pauli energies, an exact condition not met by the common choice $\rho_0 = N/V$.

A significant benefit of our approach has gone unmentioned until now. It is that the ρ_0 prescriptions we have studied obviate the limitation of Wang-Teter–type functionals to periodic systems. Any one of DEN, KIN, or ENE is well defined for isolated molecules. The opportunity provided by that generality remains to be explored.

An important question regards the general applicability of the strategy discussed in this work, as in practice one would need to run conventional (explicitly orbital-dependent) KS-DFT calculations to impose any of the constraints for ENE, DEN, and KIN. In the era of machine learning and data-driven models, this work proposes one way to build or improve nonlocal KEDFs with a density-independent kernel using information extracted from conventional KS-DFT. To build a proper model, one would need to set up a supervised learning procedure mapping ρ_0 with the density [i.e., $n(\mathbf{r}) \longleftrightarrow \rho_0$] or the nuclear geometry [i.e., $v_{\text{ext}}(\mathbf{r}) \longleftrightarrow \rho_0$] in the form of typical descriptors [50]. Such an effort would rest on the strong proof-of-principle results presented in this work. We leave it for a followup work.

Another observation is that a ρ_0 value that is appropriate for a cell containing a small number of atoms cannot be appropriate for a large cell with very many atoms where these can arrange in many ways with many different local symmetries. Clearly, a better choice would be a domain dependent ρ_0 much in the spirit of nonlocal functionals with density-dependent kernels [28–31]. An opportunity lies in the fact that there is, as yet, no unique or preferred way of determining the kernel density dependence. Thus, this work should guide future developments of KEDFs with density-dependent kernels.

ACKNOWLEDGMENTS

For the authors at Rutgers, this material is based upon work supported by the U.S. National Science Foundation under Grants No. CHE-2136142, No. CHE-2154760, and No. OAC-2321103. The work of S.B.T. was supported as part of the Center for Molecular Magnetic Quantum Materials, an Energy Frontier Research Center funded by the U.S. Department of Energy, Office of Science, Basic Energy Sciences, under Award No. DE-SC0019330.

APPENDIX A: DENSITY SCALING OF WT-LIKE KEDFs

1. Background

To determine the density scaling relations of a functional of the density, it is required to evaluate the functional for the scaled density

$$n_\lambda(\mathbf{r}) = \lambda^3 n(\lambda \mathbf{r}). \tag{A1}$$

For the noninteracting kinetic energy, it was proved [35]

$$T_s[n_\lambda] = \lambda^2 T_s[n]. \tag{A2}$$

2. Scaling relations for the nonlocal WT functional and similar

General WT-like functional with density-independent kernel is of the form

$$T_{\text{WT}}[n] = \int_V d\mathbf{r}\, d\mathbf{r}' \frac{1}{\rho_0^{(\alpha+\beta-\xi)}} \omega\left(\rho_0^{1/3}|\mathbf{r}-\mathbf{r}'|\right) n^\alpha(\mathbf{r}) n^\beta(\mathbf{r}'), \tag{A3}$$

where $\rho_0 = \frac{\int n(\mathbf{r}) d\mathbf{r}}{V}$, $\xi = \frac{5}{3}$ for SM [18], WT [17], Perrot [19], MGP [25], and WGC [16] [see WT kernel in Eq. (13) and the inverse Lindhard function in Eq. (12)] but in principle can have any value. In the following, $\kappa = \alpha + \beta$

and $\mathbf{z} = \lambda\mathbf{r}$:

$$\begin{aligned} T_{\mathrm{WT}}[n_\lambda] &= \int_V d\mathbf{r}\, d\mathbf{r}' \frac{1}{\rho_{0\lambda}^{(\kappa-\xi)}} \omega\big(\rho_{0\lambda}^{1/3}|\mathbf{r}-\mathbf{r}'|\big) n_\lambda^\alpha(\mathbf{r}) n_\lambda^\beta(\mathbf{r}') \\ &= \int_{V_\lambda} d\mathbf{r}\, d\mathbf{r}' \frac{1}{\lambda^{3\kappa-3\xi}\rho_0^{(\kappa-\xi)}} \\ &\quad \times \omega\big(\lambda\rho_0^{1/3}|\mathbf{r}-\mathbf{r}'|\big)\lambda^{3\kappa} n^\alpha(\lambda\mathbf{r}) n^\beta(\lambda\mathbf{r}') \\ &= \int_V d\mathbf{z}\, d\mathbf{z}' \omega\left(\lambda\rho_0^{1/3}\frac{|\mathbf{z}-\mathbf{z}'|}{\lambda}\right)\lambda^{3\xi-6} n^\alpha(\mathbf{z}) n^\beta(\mathbf{z}') \\ &= \lambda^{3\xi-6}\int_V d\mathbf{z}\, d\mathbf{z}' \omega\big(\rho_0^{1/3}|\mathbf{z}-\mathbf{z}'|\big) n^\alpha(\mathbf{z}) n^\beta(\mathbf{z}') \\ &= \lambda^{3\xi-6} T_{\mathrm{WT}}[n], \end{aligned} \tag{A4}$$

where $V_\lambda = \frac{V}{\lambda^3}$ The foregoing result shows that the correct scaling relations are recovered for $\xi = \frac{8}{3}$ and for any value of κ.

Unfortunately, KEDFs like WT, WGC, SM, MGP, and Perrot use $\xi = \frac{5}{3}$, and hence violate the scaling relations by scaling like λ^{-1}. The SCA functional introduced in Eq. (21) by multiplying the WT kernel effectively by N/V results in a correct λ^2 scaling.

APPENDIX B: BEHAVIOR OF THE WT KERNEL AS $\rho_0 \to 0$

As ρ_0 approaches zero, the WT kernel tends to

$$\begin{aligned} \tilde{w}(\mathbf{q}) &= \frac{5\left[\left(\frac{1}{2}+\frac{1-\eta^2}{4\eta}\ln\left|\frac{1+\eta}{1-\eta}\right|\right)^{-1} - 3\eta^2 - 1\right]}{9\alpha\beta\rho_0^{\alpha+\beta-\frac{5}{3}}} \\ &\to -\frac{8}{9\alpha\beta\rho_0^{\alpha+\beta-\frac{5}{3}}}\left(1+\frac{24}{175}\frac{1}{\eta^2}+O(\eta^{-4})\right) \\ &= -1.28\left(1+\frac{24}{175}\frac{1}{\eta^2}+O(\eta^{-4})\right). \end{aligned} \tag{B1}$$

The above shows that the WT Pauli energy would go to $-0.28\,T_{\mathrm{TF}}$ should $\rho_0 \to 0$. Thus, in this limit, the WT functional violates the Pauli energy positivity condition. This result is used to aid the discussion of the helium atom results in the text.

[1] E. A. Carter, Challenges in modeling materials properties without experimental input, Science **321**, 800 (2008).

[2] W. Kohn and L. J. Sham, Self-consistent equations including exchange and correlation effects, Phys. Rev. **140**, A1133 (1965).

[3] J. P. Perdew, My life in science: Lessons for yours? J. Chem. Phys. **160**, 010402 (2024).

[4] E. Prodan and W. Kohn, Nearsightedness of electronic matter, Proc. Natl. Acad. Sci. USA **102**, 11635 (2005).

[5] W. Kohn, Density functional and density matrix method scaling linearly with the number of atoms, Phys. Rev. Lett. **76**, 3168 (1996).

[6] S. Goedecker, Linear scaling electronic structure methods, Rev. Mod. Phys. **71**, 1085 (1999).

[7] W. Mi, K. Luo, S. B. Trickey, and M. Pavanello, Orbital-free density functional theory: An attractive electronic structure method for large-scale first-principles simulations, Chem. Rev. **123**, 12039 (2023).

[8] L. H. Thomas, The calculation of atomic fields, in *Mathematical Proceedings of the Cambridge Philosophical Society* (Cambridge University Press, Cambridge, 1927), Vol. 23, pp. 542–548.

[9] C. F. v. Weizsäcker, Zur theorie der kernmassen, Z. Phys. **96**, 431 (1935).

[10] H. Lee, C. Lee, and R. G. Parr, Conjoint gradient correction to the Hartree-Fock kinetic- and exchange-energy density functionals, Phys. Rev. A **44**, 768 (1991).

[11] K. Luo, V. V. Karasiev, and S. B. Trickey, A simple generalized gradient approximation for the noninteracting kinetic energy density functional, Phys. Rev. B **98**, 041111(R) (2018).

[12] L. A. Constantin, E. Fabiano, and F. Della Sala, Semilocal Pauli–Gaussian kinetic functionals for orbital-free density functional theory calculations of solids, J. Phys. Chem. Lett. **9**, 4385 (2018).

[13] S. Manzhos, J. Lüder, and M. Ihara, Machine learning of kinetic energy densities with target and feature smoothing: Better results with fewer training data, J. Chem. Phys. **159** (2023).

[14] M. Levy and J. P. Perdew, Density functionals for exchange and correlation energies: Exact conditions and comparison of approximations, Int. J. Quantum Chem. **49**, 539 (1994).

[15] J. Sun, A. Ruzsinszky, and J. P. Perdew, Strongly constrained and appropriately normed semilocal density functional, Phys. Rev. Lett. **115**, 036402 (2015).

[16] Y. A. Wang, N. Govind, and E. A. Carter, Orbital-free kinetic-energy density functionals with a density-dependent kernel, Phys. Rev. B **60**, 16350 (1999).

[17] L.-W. Wang and M. P. Teter, Kinetic-energy functional of the electron density, Phys. Rev. B **45**, 13196 (1992).

[18] E. Smargiassi and P. A. Madden, Orbital-free kinetic-energy functionals for first-principles molecular dynamics, Phys. Rev. B **49**, 5220 (1994).

[19] F. Perrot, Hydrogen-hydrogen interaction in an electron gas, J. Phys.: Condens. Matter **6**, 431 (1994).

[20] J. Lindhard, On the properties of a gas of charged particles, Kgl. Danske Videnskab. Selskab Mat.-Fys. Medd. **28** (1954).

[21] Y. A. Wang and E. A. Carter, Orbital-free kinetic-energy density functional theory, *Theoretical Methods in Condensed Phase Chemistry*, edited by S. Schwartz (Springer Netherlandser, Dordrech, 2000), Chap. 5, pp. 117–184.

[22] L. A. Constantin, E. Fabiano, and F. Della Sala, Performance of semilocal kinetic energy functionals for orbital-free density functional theory, J. Chem. Theory Comput. **15**, 3044 (2019).

[23] Z. A. Moldabekov, X. Shao, M. Pavanello, J. Vorberger, F. Graziani, and T. Dornheim, Imposing correct jellium response is key to predict the density response by orbital-free dft, Phys. Rev. B **108**, 235168 (2023).

[24] Y. A. Wang, N. Govind, and E. A. Carter, Orbital-free kinetic-energy functionals for the nearly free electron gas, Phys. Rev. B **58**, 13465 (1998).
[25] W. Mi, A. Genova, and M. Pavanello, Nonlocal kinetic energy functionals by functional integration, J. Chem. Phys. **148**, 184107 (2018).
[26] L. A. Constantin, E. Fabiano, and F. Della Sala, Nonlocal kinetic energy functional from the jellium-with-gap model: Applications to orbital-free density functional theory, Phys. Rev. B **97**, 205137 (2018).
[27] W. Mi and M. Pavanello, Orbital-free density functional theory correctly models quantum dots when asymptotics, nonlocality, and nonhomogeneity are accounted for, Phys. Rev. B **100**, 041105(R) (2019).
[28] W. Mi and M. Pavanello, Nonlocal subsystem density functional theory, J. Phys. Chem. Lett. **11**, 272 (2020).
[29] C. Huang and E. A. Carter, Nonlocal orbital-free kinetic energy density functional for semiconductors, Phys. Rev. B **81**, 045206 (2010).
[30] X. Shao, W. Mi, and M. Pavanello, Revised Huang-Carter nonlocal kinetic energy functional for semiconductors and their surfaces, Phys. Rev. B **104**, 045118 (2021).
[31] Q. Xu, Y. Wang, and Y. Ma, Nonlocal kinetic energy density functional via line integrals and its application to orbital-free density functional theory, Phys. Rev. B **100**, 205132 (2019).
[32] E. Chacón, J. E. Alvarellos, and P. Tarazona, Nonlocal kinetic energy functional for nonhomogeneous electron systems, Phys. Rev. B **32**, 7868 (1985).
[33] X. Blanc and E. Cancès, Nonlinear instability of density-independent orbital-free kinetic-energy functionals, J. Chem. Phys. **122**, 214106 (2005).
[34] W. C. Witt, B. W. B. Shires, C. W. Tan, W. J. Jankowski, and C. J. Pickard, Random structure searching with orbital-free density functional theory, J. Phys. Chem. A **125**, 1650 (2021).
[35] M. Levy and J. P. Perdew, Hellmann-Feynman, virial, and scaling requisites for the exact universal density functionals. shape of the correlation potential and diamagnetic susceptibility for atoms, Phys. Rev. A **32**, 2010 (1985).
[36] A. B. Alchagirov, J. P. Perdew, J. C. Boettger, R. C. Albers, and C. Fiolhais, Reply to "comment on 'energy and pressure versus volume: Equations of state motivated by the stabilized jellium model'", Phys. Rev. B **67**, 026103 (2003).
[37] C. Huang and E. A. Carter, Toward an orbital-free density functional theory of transition metals based on an electron density decomposition, Phys. Rev. B **85**, 045126 (2012).
[38] S. Wang and H. Ye, *Ab initio* elastic constants for the lonsdaleite phases of C, Si and Ge, J. Phys.: Condens. Matter **15**, 5307 (2003).
[39] X. He, M. Li, C. Rong, D. Zhao, W. Liu, P. W. Ayers, and S. Liu, Some recent advances in density-based reactivity theory [J. Phys. Chem. A (to be published)].
[40] X. Shao, O. Andreussi, D. Ceresoli, M. Truscott, A. Baczewski, Q. Campbell, and M. Pavanello, QEpy: Quantum ESPRESSO in Python, https://gitlab.com/shaoxc/qepy.
[41] X. Shao, K. Jiang, W. Mi, A. Genova, and M. Pavanello, DFTpy: An efficient and object-oriented platform for orbital-free DFT simulations, WIREs: Comput. Mol. Sci. **11**, e1482 (2021).
[42] B. Zhou, Y. A. Wang, and E. A. Carter, Transferable local pseudopotentials derived via inversion of the Kohn-Sham equations in a bulk environment, Phys. Rev. B **69**, 125109 (2004).
[43] J. P. Perdew and A. Zunger, Self-interaction correction to density-functional approximations for many-electron systems, Phys. Rev. B **23**, 5048 (1981).
[44] H. J. Monkhorst and J. D. Pack, Special points for Brillouin-zone integrations, Phys. Rev. B **13**, 5188 (1976).
[45] J. D. Pack and H. J. Monkhorst, "Special points for Brillouin-zone integrations"—a reply, Phys. Rev. B **16**, 1748 (1977).
[46] V. Rios, X. Shao, and M. Pavanello, WT: Kinetic energy density functional, https://github.com/ValeriaRV99/wt.
[47] M.-C. Kim, E. Sim, and K. Burke, Understanding and reducing errors in density functional calculations, Phys. Rev. Lett. **111**, 073003 (2013).
[48] M. Levy and H. Ou-Yang, Exact properties of the Pauli potential for the square root of the electron density and the kinetic energy functional, Phys. Rev. A **38**, 625 (1988).
[49] See Supplemental Material at http://link.aps.org/supplemental/10.1103/PhysRevB.110.085129 for additional details, tables and figures regarding the Hartree self-energy of the Fukui functions, energy response, KEDF response, and Pauli energy values.
[50] L. Himanen, M. O. J. Jäger, E. V. Morooka, F. Federici Canova, Y. S. Ranawat, D. Z. Gao, P. Rinke, and A. S. Foster, DScribe: Library of descriptors for machine learning in materials science, Comput. Phys. Commun. **247**, 106949 (2020).